Spectral Graph Partitioning and Its Application in Wildfire Analysis

Jacob Lee

Abstract

Spectral graph theory studies the relationship between the graph structure and the eigenvalues of matrices associated with graphs. Among these matrices, the graph Laplacian plays a central role in understanding connectivity, diffusion processes, and graph partitioning. In this paper, we investigate the second-smallest Laplacian eigenvalue, known as the Fiedler value, and the corresponding Fiedler vector. We develop the theoretical foundations of Fiedler partitioning through the Rayleigh quotient characterization of eigenvalues and examine how the sign structure of Fiedler vectors reveals sparse weak points within graphs. Several classical graph families are analyzed to illustrate these properties. Finally, we discuss applications of spectral partitioning to spatial network design and urban wildfire mitigation. Ultimately, this work contributes to a spectral-based strategy for optimizing firebreak placements.

1 Introduction

In many complex network systems, a fundamental challenge is to partition a large graph into highly cohesive subgraphs while minimizing the number of intersecting edges between them. This challenge, known as the graph partitioning problem, is central to numerous domains. In social network analysis, it enables community detection; in VLSI circuit design, it optimizes microchip layouts; and in environmental engineering, it identifies optimal boundaries for landscape-level interventions. Spectral partitioning methods resolve these discrete optimization problems by leveraging the continuous properties of matrix eigenvalues and eigenvectors, effectively mapping physical network characteristics to algebraic variables.

The origins of graph theory date back to 1736 when Leonhard Euler solved the famous Seven Bridges of Königsberg problem, introducing the idea of representing physical locations as vertices and the paths connecting them as edges. His solution established graph theory as a branch of discrete mathematics and demonstrated that many seemingly complex problems could be analyzed through abstract mathematical structures rather than geometric measurements. During the nineteenth century, the field continued to develop through the work of Gustav Kirchhoff, who introduced what is now known as the Matrix-Tree Theorem in 1847. His work with the Laplacian matrix provided one of the earliest and most significant connections between graph theory and linear algebra. This discovery laid the groundwork for representing graphs using matrices, allowing mathematicians to study graph structure through algebraic methods.

The modern era of spectral graph theory emerged in the latter half of the twentieth century through the pioneering work of Miroslav Fiedler. In a series of influential papers, Fiedler demonstrated that the second-smallest eigenvalue of the Laplacian matrix provides a quantitative measure of a graph's connectivity, a quantity now known as the algebraic connectivity of the graph. He further showed that the corresponding eigenvector, now called the Fiedler vector, naturally partitions a graph into highly connected subgraphs while separating weakly connected regions. These discoveries established the mathematical foundation for spectral partitioning algorithms, which remain among the most important techniques in graph clustering and network optimization. Building upon Fiedler's work, researchers including Fan Chung, Chris Godsil, Gordon Royle, and Daniel Spielman significantly expanded the field by connecting spectral graph theory with probability theory, optimization, random walks, theoretical computer science, and network science.

The primary contributions of this paper are threefold:

Foundation: We provide self-contained, rigorous proofs for the foundational properties of the graph Laplacian matrix.

Classification: We evaluate the sign structures of Fiedler vectors across diverse graph families to demonstrate how topology dictates sparse cuts.

Application to Wildfire: We formalize an algorithm that reflects physical forests, using the Fiedler vector to pinpoint optimal firebreak locations.

2 Preliminaries

We first must establish formal discrete definitions and theorems.

Definition 2.1 (Graphs)**.** A graph $G = (V, E)$ consists of a finite set of vertices $V = \{v_1, \ldots, v_n\}$ and a set of edges $E \subseteq V \times V$, where each element $\{v_i, v_j\} \in E$ represents a connection between v_i and v_j. Alternatively, a network can be parameterized via a symmetric weight matrix $W \in \mathbb{R}^{n\times n}$, where $W_{ij} \geq 0$ denotes the specific value or significance of the edge between v_i and v_j. In this work, we assume G is undirected ($W_{ij} = W_{ji}$) and contains no self-loops ($W_{ii} = 0$).

Definition 2.2 (Neighborhood)**.** For any vertex v in a graph G, the *open neighborhood* is denoted as $N(v)$, which consists of all vertices adjacent to v. The *closed neighborhood* is defined as:

$$N[v] = N(v) \cup \{v\}$$

Definition 2.3 (Subgraphs and Induced Subgraphs)**.** A graph $H = (W, F)$ is a *subgraph* of $G = (V, E)$ if $W \subseteq V$ and $F \subseteq E$. It is an *induced subgraph* (written $H \triangleleft G$) if F contains all edges from G that connect vertices in W.

Definition 2.4 (Bipartiteness)**.** A graph is *bipartite* if its vertices can be partitioned into two independent sets. A graph is bipartite if and only if it contains no odd-length cycles.

Definition 2.5 (Domination Number)**.** The *domination number*, denoted $\gamma(G)$, is the minimum size of a vertex set S such that every vertex outside S is adjacent to at least one member of S.

Definition 2.6 (Dimension Formula)**.** For two subspaces U and W of a vector space, their dimensions interact according to the formula:

$$\dim(U + W) = \dim(U) + \dim(W) - \dim(U \cap W)$$

Definition 2.7 (Transpose)**.** The *transpose* of a matrix M, denoted M^T, is formed by swapping rows and columns ($M^T_{ij} = M_{ji}$). It follows the reversal rule for products:

$$(AB)^T = B^T A^T$$

Definition 2.8 (Symmetry)**.** A matrix M is *symmetric* if $M = M^T$. Real symmetric matrices strictly possess real eigenvalues.

Theorem 2.9 *(Spectral Theorem).* Let $M \in \mathbb{R}^{n\times n}$ be a real symmetric matrix ($M = M^T$). Then:

1. All eigenvalues $\lambda_1, \lambda_2, \ldots, \lambda_n$ of M are real numbers ($\lambda_i \in \mathbb{R}$).
2. There exists an orthonormal basis of $\mathbb{R}^n$ consisting of eigenvectors $x_1, x_2, \ldots, x_n$ of M, such that $x_i^T x_j = 0$ for all $i \neq j$.
3. M can be factored into the spectral decomposition $M = Q\Lambda Q^T$, where Q is an orthogonal matrix ($Q^T Q = I$) and $\Lambda = \text{diag}(\lambda_1, \ldots, \lambda_n)$.

3 Matrix and Graph Laplacian

A graph of any structure can be represented with a Laplacian graph.

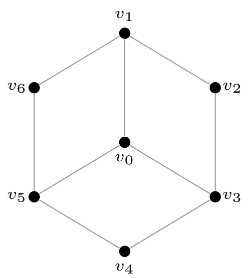

Figure 1: A simple graph of 7 vertices.

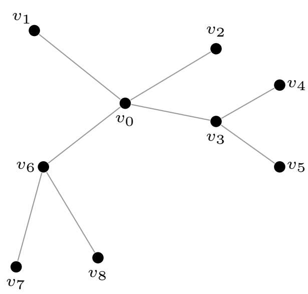

Figure 2: An acyclic tree graph of 9 vertices.

3.1 Adjacency Matrices

For an unweighted graph $G = (V, E)$ with $|V| = n$, the adjacency matrix $A \in \{0,1\}^{n\times n}$ is a binary symmetric matrix defined as:

$$A_{ij} = \begin{cases} 1 & \text{if } \{v_i, v_j\} \in E, \\ 0 & \text{otherwise.} \end{cases} \tag{1}$$

For a weighted graph $G = (V, E, W)$ where $W : E \to \mathbb{R}$ maps edges to real-valued weights, the weighted adjacency matrix $W \in \mathbb{R}^{n\times n}$ is defined as:

$$W_{ij} = \begin{cases} w(v_i, v_j) & \text{if } \{v_i, v_j\} \in E, \\ 0 & \text{otherwise.} \end{cases} \tag{2}$$

3.2 Degree Matrices

The degree matrix $D \in \mathbb{R}^{n\times n}$ is a diagonal matrix defined as:

$$D_{ii} = \sum_{j=1}^{n} W_{ij} \tag{3}$$

where $D_{ij} = 0$ for all $i \neq j$. For an unweighted graph, this simplifies via the binary adjacency matrix to:

$$D_{ii} = \sum_{j=1}^{n} A_{ij} = \deg(v_i) \tag{4}$$

$$A = \begin{bmatrix} 0 & 1 & 0 & 1 & 0 & 1 & 0 \\ 1 & 0 & 1 & 0 & 0 & 0 & 1 \\ 0 & 1 & 0 & 1 & 0 & 0 & 0 \\ 1 & 0 & 1 & 0 & 1 & 0 & 0 \\ 0 & 0 & 0 & 1 & 0 & 1 & 0 \\ 1 & 0 & 0 & 0 & 1 & 0 & 1 \\ 0 & 1 & 0 & 0 & 0 & 1 & 0 \end{bmatrix}$$

Adjacency Matrix of Figure 1

$$D = \begin{bmatrix} 3 & 0 & 0 & 0 & 0 & 0 & 0 \\ 0 & 3 & 0 & 0 & 0 & 0 & 0 \\ 0 & 0 & 2 & 0 & 0 & 0 & 0 \\ 0 & 0 & 0 & 3 & 0 & 0 & 0 \\ 0 & 0 & 0 & 0 & 2 & 0 & 0 \\ 0 & 0 & 0 & 0 & 0 & 3 & 0 \\ 0 & 0 & 0 & 0 & 0 & 0 & 2 \end{bmatrix}$$

Degree Matrix of Figure 1

3.3 Graph Laplacian

Now, given both the degree and adjacency matrices, we define the graph Laplacian matrix $L \in \mathbb{R}^{n\times n}$ as:

$$L = D - A \tag{5}$$

For weighted graphs, the elements are mapped directly as:

$$L_{ij} = \begin{cases} \sum_{k\neq i} W_{ik} & \text{if } i = j \\ -W_{ij} & \text{if } i \neq j \end{cases} \tag{6}$$

L tracks network structure by subtracting the connection layout (A) from each node's total connection count (D). This operation creates a matrix where the diagonal entries show the degrees of the vertices and the off-diagonal entries mark edge paths with negative values. It reveals the entire topology of the graph.

$$L = \begin{bmatrix} 3 & -1 & 0 & -1 & 0 & -1 & 0 \\ -1 & 3 & -1 & 0 & 0 & 0 & -1 \\ 0 & -1 & 2 & -1 & 0 & 0 & 0 \\ -1 & 0 & -1 & 3 & -1 & 0 & 0 \\ 0 & 0 & 0 & -1 & 2 & -1 & 0 \\ -1 & 0 & 0 & 0 & -1 & 3 & -1 \\ 0 & -1 & 0 & 0 & 0 & -1 & 2 \end{bmatrix}$$

Laplacian Matrix of Figure 1

The above confirms that Figure 1 is a single fully connected network because it contains exactly one zero eigenvalue. Looking along the main diagonal, we can read the exact connection count for each vertex: nodes v_0, v_1, v_3, and v_5 are highly connected hubs each touching 3 edges, while nodes v_2, v_4, and v_6 are peripheral points with only 2 edges. The negative ones scattered throughout the rest of the grid perfectly map out the outer boundary ring (v_1 to v_2 to v_3 and so on) and highlight the central node v_0.

4 Fundamental Properties of the Graph Laplacian

Before diving into the core of the graph partitioning, we must establish several properties of the Laplacian operator.

Because all graphs are undirected ($W_{ij} = W_{ji}$), both D and A are symmetric matrices. It follows directly that $L = D - A$ is symmetric ($L^T = L$). By the spectral theorem for symmetric matrices, the eigenvalues of L are all real ($\lambda_i \in \mathbb{R}$), and its eigenvectors form a complete orthonormal basis across $\mathbb{R}^n$.

Theorem 4.1. The graph Laplacian matrix L is positive semidefinite.

Proof. A matrix L is positive semidefinite if and only if for any $x \in \mathbb{R}^n$, the quadratic form evaluates as non-negative: $x^T L x \geq 0$. Expanding the quadratic form shows:

$$x^T L x = x^T D x - x^T A x = \sum_{i \in V} D_{ii} x_i^2 - \sum_{i,j \in V} A_{ij} x_i x_j$$

Leveraging the property that $D_{ii} = \sum_j W_{ij}$, we substitute and combine terms across each connected edge:

$$x^T L x = \sum_{i \in V} \sum_{j \in V} W_{ij} x_i^2 - \sum_{i,j \in V} W_{ij} x_i x_j = \frac{1}{2} \sum_{i,j \in V} W_{ij}(x_i^2 - 2x_i x_j + x_j^2)$$

Grouping the algebraic squares yields the final quadratic expression:

$$x^T L x = \sum_{\{v_i, v_j\} \in E} W_{ij}(x_i - x_j)^2 \tag{7}$$

Because the weights $W_{ij} \geq 0$ and the squared term $(x_i - x_j)^2 \geq 0$ for all real parameters, the final summation must evaluate to a value greater than or equal to 0. Thus, L is positive semidefinite. □

Theorem 4.2. The algebraic expression $x^T L x = \sum_{\{v_i, v_j\} \in E} W_{ij}(x_i - x_j)^2$ acts as a discrete Dirichlet energy function over the graph network.

Proof. This follows directly from expanding the summation over all distinct vertex boundaries, as proven in Theorem 4.1. The quadratic form effectively maps structural distance: if two vertices share a strong, highly weighted connection ($W_{ij} \gg 0$), the optimization engine assigns them similar values ($x_i \approx x_j$) to minimize total network energy. □

Given that L is positive semidefinite, its real eigenvalues can be sorted in ascending order:

$$0 = \lambda_1 \leq \lambda_2 \leq \cdots \leq \lambda_n \tag{8}$$

The absolute minimum eigenvalue λ_1 is always identically equal to 0. This trivial solution corresponds to the all-ones constant vector $\mathbf{1} = [1, 1, \ldots, 1]^T$, because multiplying any row of L by a constant vector yields zero ($L\mathbf{1} = \mathbf{0}$), showing that the row sums of any graph Laplacian are zero.

5 Algebraic Connectivity and Network Robustness

The second-smallest eigenvalue, λ_2, represents a foundational structural metric in spectral graph theory, serving as a master variable between discrete geometry and linear algebra.

Theorem 5.1. The geometric multiplicity of the zero eigenvalue ($\lambda = 0$) matches the exact number of disjoint connected components contained within graph G.

Proof. Suppose graph G consists of k completely disconnected subgraphs $\{G_1, G_2, \ldots, G_k\}$. We can construct k independent indicator vectors $x^{(1)}, \ldots, x^{(k)}$ such that:

$$x_i^{(m)} = \begin{cases} 1 & \text{if } v_i \in G_m \\ 0 & \text{otherwise} \end{cases}$$

Evaluating the Dirichlet quadratic form for any indicator vector yields $x^{(m)T} L x^{(m)} = \sum W_{ij}(x_i - x_j)^2 = 0$, since no active edge bridges separate components ($W_{ij} = 0$ whenever $v_i \in G_m$ and $v_j \notin G_m$). Because these k vectors have disjoint supports, they are linearly independent. Thus, the nullspace of L has a dimension equal to k. □

Connectivity Criterion

Theorem 5.2 (Miroslav Fiedler, 1973)**.** A network graph G is a single, fully connected component if and only if the second-smallest Laplacian eigenvalue is strictly positive ($\lambda_2 > 0$).

Proof. By Theorem 5.1, the number of zero eigenvalues equals the number of connected components. If G is fully connected, it forms exactly one component, meaning the eigenvalue $\lambda_1 = 0$ must have a multiplicity of exactly 1. Consequently, the next consecutive eigenvalue in the ordered spectrum must satisfy $\lambda_2 > 0$. □

The value λ_2 is defined as the *algebraic connectivity* or *Fiedler value* of the graph. It measures the global structural integrity and communication speed of a network:

- **Low Algebraic Connectivity ($\lambda_2 \to 0^+$):** Indicates a highly vulnerable network featuring severe topological bottlenecks. The graph contains fragile cutpoints where the removal of only a few weak edges can cleanly slice the system into separate components.
- **High Algebraic Connectivity ($\lambda_2 \gg 0$):** Indicates an expansive, highly interconnected topology (e.g., expander graphs or complete networks). Such networks lack singular choke points, making them highly resilient against localized structural disruptions.

6 Variational Characterization and the Rayleigh Quotient

To find λ_2 without expensive global matrix inversions, we look at the problem through variational optimization.

For any non-zero coordinate vector $x \in \mathbb{R}^n$, the Rayleigh Quotient $R(L, x)$ maps a continuous scaling factor across the Laplacian matrix:

$$R(L, x) = \frac{x^T L x}{x^T x} = \frac{\sum_{\{v_i, v_j\} \in E} W_{ij}(x_i - x_j)^2}{\sum_{i \in V} x_i^2} \tag{9}$$

The Rayleigh quotient measures the ratio of total network "strain" or coordinate divergence across edges relative to the total variance of the coordinates assigned to the vertices.

Because the absolute minimum eigenvalue $\lambda_1 = 0$ corresponds to the trivial constant eigenvector $x_1 = \mathbf{1}$, we can isolate the algebraic connectivity value λ_2 by minimizing the Rayleigh quotient across a restricted subspace.

Theorem 6.1. The algebraic connectivity λ_2 satisfies the constrained optimization problem:

$$\lambda_2 = \min_{x \perp \mathbf{1}, x \neq \mathbf{0}} \frac{x^T L x}{x^T x} \tag{10}$$

Proof. By the spectral theorem, we expand any real vector $x \in \mathbb{R}^n$ as a linear combination of the orthonormal eigenvectors of L, denoted $\{x_1, x_2, \ldots, x_n\}$, such that $x = \sum_{i=1}^n c_i x_i$. The orthogonality constraint $x \perp \mathbf{1}$ dictates that the dot product $x \cdot x_1 = 0$, forcing the first coefficient to zero ($c_1 = 0$). Substituting this expansion into the Rayleigh quotient yields:

$$\frac{x^T L x}{x^T x} = \frac{\sum_{i=2}^n \lambda_i c_i^2}{\sum_{i=2}^n c_i^2}$$

Because the eigenvalues are ordered ($\lambda_2 \leq \lambda_3 \leq \cdots \leq \lambda_n$), we can establish a strict lower bound by substituting λ_2 for all terms:

$$\frac{\sum_{i=2}^n \lambda_i c_i^2}{\sum_{i=2}^n c_i^2} \geq \frac{\sum_{i=2}^n \lambda_2 c_i^2}{\sum_{i=2}^n c_i^2} = \lambda_2$$

This lower bound is exactly reached when we choose $c_2 = 1$ and $c_i = 0$ for all $i > 2$, which corresponds to setting $x = x_2$. This completes the proof. □

7 Fiedler Vectors and Coordinate Projections

The specific eigenvector $x_2 \in \mathbb{R}^n$ that satisfies the minimization problem in Theorem 6.1 is known as the *Fiedler vector*.

7.1 Sign-Structure Constraints

By definition, the Fiedler vector must sit perfectly orthogonal to the trivial constant vector ($x_2 \perp \mathbf{1}$). This orthogonality constraint manifests as a zero-sum balance requirement across the vector entries:

$$x_2 \cdot \mathbf{1} = \sum_{i=1}^{n} (x_2)_i = 0 \tag{11}$$

Consequently, except for the trivial case where all elements are zero, the Fiedler vector must contain both strictly positive and strictly negative entries. This mathematical requirement provides a natural geometric splitting mechanism.

7.2 One-Dimensional Geometric Mapping

The entries of the Fiedler vector function as an optimized one-dimensional coordinate mapping of the graph's higher-dimensional topology. By minimizing the quadratic distance objective $\sum W_{ij}(x_i - x_j)^2$, the algorithm maps tightly cohesive clusters to similar spectral coordinates. Vertices separated by fragile structural bottlenecks are pushed to opposite extremes of the real line, receiving highly divergent values and distinct algebraic signs.

8 Nodal Domains of Fiedler Vectors

Before executing discrete cuts, we analyze the spatial behavior of these spectral signs through the framework of nodal domains.

Definition 8.1 (Nodal Domain)**.** A **maximal nodal domain** of a graph vector x is a maximal, fully connected subgraph of G whose vertices all share the same sign property (i.e., all entries are strictly positive $x_i > 0$ or all entries are non-positive $x_i \leq 0$).

Theorem 8.2 (Discrete Courant Nodal Domain Theorem)**.** For any connected graph, the Fiedler vector x_2 generates at most two distinct nodal domains.

Proof. This is a discrete variation of Courant's foundational wave-equation theorem applied to matrices. For the k^{th} ordered eigenvalue of a generalized Laplacian, the number of distinct sign-consistent connected components cannot exceed k. For the second eigenvalue ($k = 2$), the graph is naturally divided into at most 2 sign-consistent connected subgraphs. □

This mathematical guarantee underpins spectral partitioning. It ensures that splitting a network based on Fiedler vector signs will partition the network into two cohesive blocks, rather than fracturing it into a chaotic collection of scattered, isolated components.

9 Spectral Graph Partitioning Theory

The theoretical properties established above provide a rigorous foundation for a formal, discrete spectral graph partitioning algorithm.

9.1 Sign-Based Partition Matrices

The global vertex set V can be partitioned into two disjoint, highly cohesive subgraphs, V_+ and V_-, by evaluating the algebraic sign of each vertex entry in the Fiedler vector:

$$V_+ = \{v_i \in V : (x_2)_i > 0\}, \quad V_- = \{v_i \in V : (x_2)_i \leq 0\} \tag{12}$$

9.2 The Discrete Ratio Cut Objective

This sign-splitting method provides a continuous relaxation for NP-hard discrete optimization problems. Specifically, it approximates the minimization of the global *Ratio Cut* (RCut), which measures the ratio of severed edge boundaries relative to the size of the resulting clusters:

$$\mathrm{RCut}(V_+, V_-) = \sum_{v_i \in V_+, v_j \in V_-} W_{ij} \left(\frac{1}{|V_+|} + \frac{1}{|V_-|} \right) \tag{13}$$

The continuous coordinates of the Fiedler vector serve as an optimized surrogate, grouping heavily linked nodes together while isolating and severing the weakest structural bridges.

10 Graph Families

To verify how different structures influence algebraic connectivity and the shape of the Fiedler vector, we analyze four classical graph families.

Table 1: Spectral Profiles of Classical Unweighted Graph Families (n Vertices)

Graph Family	**Fiedler Value** (λ_2)	**Bottleneck Level**	**Vector Trajectory**
Path (P_n)	$2\left(1 - \cos\frac{\pi}{n}\right) \approx \frac{\pi^2}{n^2}$	Extreme Vulnerability	Linear Monotonic Gradient
Cycle (C_n)	$2\left(1 - \cos\frac{2\pi}{n}\right) \approx \frac{4\pi^2}{n^2}$	Moderate Multi-Path	Symmetric Sinusoidal Wave
Complete (K_n)	n	Absolute Resilience	Degenerate Equidistant Splits
Star (S_n)	1	Centralized Hub	Bipolar Outer Leaf Clusters

10.1 Path Graphs (P_n)

A path graph represents a highly fragile string of connections. The algebraic connectivity scales inversely with the square of the size of the graph: $\lambda_2 \approx \frac{\pi^2}{n^2}$. As $n \to \infty$, λ_2 approaches 0, indicating extreme structural vulnerability. The Fiedler vector follows a smooth, monotonic gradient from negative values at one end to positive values at the other, placing the zero-crossing cut directly across the central edge.

10.2 Cycle Graphs (C_n)

Cycle graphs form a closed loop, introducing an alternate path that doubles the algebraic connectivity relative to path graphs: $\lambda_2 \approx \frac{4\pi^2}{n^2}$. Because of the loop's geometric symmetry, the second and third eigenvalues are identical ($\lambda_2 = \lambda_3$), creating a repeated spectrum. The Fiedler vector manifests as a discrete sinusoidal wave, partitioning the ring into two equal, contiguous semicircles.

10.3 Complete Graphs (K_n)

In a complete graph, every vertex shares an active edge with every other node ($W_{ij} = 1$). This structure eliminates localized bottlenecks, yielding a maximized algebraic connectivity of $\lambda_2 = n$. Because all nodes are structurally equidistant, the Fiedler value has a multiplicity of $n - 1$. The Fiedler coordinates can split the graph across any arbitrary balanced boundary, reflecting the total structural resilience of the network.

10.4 Star Graphs (S_n)

A star graph features a single centralized hub node connected to $n - 1$ independent outer leaf vertices. This configuration yields an algebraic connectivity of exactly $\lambda_2 = 1$, independent of the network scale n. The Fiedler vector assigns a coordinate of 0 to the central hub, while dividing the outer leaf nodes into opposing positive and negative clusters. This reveals that the central hub is a critical point of vulnerability for the network.

11 Application to Urban Wildfire Networks

We can model physical environments as spatial graph networks, mapping assets (e.g., structures, dense timber plots) to vertices and localized transmission channels (e.g., canopy contiguity, ember flight trajectories) to edges. Under this paradigm, the sign structures of the Fiedler vector illuminate the critical bottlenecks governing cascading wildfire propagation. Removing a vertex or clearing fuel boundaries along the zero-crossing threshold partitions the network into disconnected components. Placing physical firebreaks systematically where the Fiedler vector changes sign maximizes structural isolation, ensuring optimal distribution of containment resources.

11.1 Phase 1: Isotropic Structural Edge Partitioning (Baseline)

The baseline formulation models the forest landscape as a static, unwarped geometric graph $G = (V, E, W)$ where edge capacities map directly to the Euclidean metric $W_{ij} = \|x_i - x_j\|_2$. We construct the combinatorial graph Laplacian matrix $L \in \mathbb{R}^{n \times n}$ as follows:

$$L_{ij} = \begin{cases} \sum_{k \neq i} W_{ik} & \text{if } i = j \\ -W_{ij} & \text{if } i \neq j \end{cases} \tag{14}$$

By invoking Courant-Fischer minimax theorem principles, minimizing the Rayleigh quotient subject to appropriate orthogonal constraints yields the Fiedler vector $v \in \mathbb{R}^n$ corresponding to the algebraic connectivity eigenvalue λ_2:

$$\lambda_2 = \min_{v \perp \mathbf{1}, \|v\|_2 = 1} v^T L v = \min_{v \perp \mathbf{1}, \|v\|_2 = 1} \sum_{(i,j) \in E} W_{ij} (v_i - v_j)^2 \tag{15}$$

Differentiating this metric yields the baseline structural interdiction score ($\mathcal{S}_{\text{base}}$) allocated to each topological vector boundary:

$$\mathcal{S}_{\text{base}}(i, j) = W_{ij} (v_i - v_j)^2 \tag{16}$$

This baseline formulation targets structural bottlenecks by evaluating the square of the difference between spectral coordinates. While mathematically robust for global graph partitioning, it is fundamentally localized-hazard-blind and cannot incorporate non-isotropic environmental threats.

11.2 Phase 2: Stationary Source-Anchored Attenuation (Model A)

To prevent the global optimization objective from allocating defensive structures at distances decoupled from the active ignition zone, we introduce a localized spatial multiplier. Let V_0 denote the absolute node origin of the ignition. We define a static localized boundary scoring metric $\mathcal{S}_{\text{static}}$ modified by a spatial decay factor:

$$\mathcal{S}_{\text{static}}(i,j) = \left[W_{ij}(v_i - v_j)^2\right] \cdot \exp\left(-\frac{\min\left(d(i,V_0), d(j,V_0)\right)}{\gamma}\right) \tag{17}$$

where $\gamma \in \mathbb{R}^+$ represents the designated containment radius scale hyperparameter and $d(a,b)$ evaluates Euclidean distance. As the spatial coordinates of edge candidates deviate from the source anchor, the exponential tracking metric drops toward zero. This mathematical modification confines the search space of the spectral clustering algorithm to an absolute radial proximity envelope centered on the initial outbreak.

11.3 Phase 3: Dynamic Perimeter Tracking Allocation (Model B)

A stationary containment solution cannot adjust as the physical fire line advances or protect the graph structure when assets are consumed. We extend the framework to a discrete time-varying regime t. Let $B_t \subset V$ signify the subset of actively burning vertices at step t, and $E_t \subset V$ represent exhausted nodes. To eliminate the allocation of containment resources to dead assets or active flames, we introduce a conditional interdiction metric:

$$\mathcal{S}_{\text{dynamic}}(i,j,t) = \begin{cases} -1 & \text{if } \{i,j\} \cap (B_t \cup E_t) \neq \emptyset \\ \mathcal{S}_{\text{base}}(i,j) \cdot \exp\left(-\frac{\text{dist}(\{i,j\},B_t)}{\gamma}\right) & \text{otherwise} \end{cases} \tag{18}$$

where the time-stepped spatial scalar evaluates the minimum instantaneous geometric distance separating candidate vector edges from the moving perimeter boundary B_t:

$$\text{dist}(\{i,j\},B_t) = \min_{u \in B_t}\left(\min\left(d(i,u), d(j,u)\right)\right) \tag{19}$$

This step links the graph partition mechanism directly to the transient states of the fire propagation engine, ensuring that containment decisions are made directly adjacent to the evolving fire front.

11.4 Phase 4: The Final Model — Predictive Decoupled Covariate Realignment

The complete framework addresses physical irregularities by fully integrating multi-layered environmental covariates: a continuous convective wind vector $\vec{w} \in \mathbb{R}^2$, a topographical elevation field $e_i \in \mathbb{R}$, a fuel biomass density layer $F_{\text{fuel}} \in \mathbb{R}^+$, and an intrinsic species flammability scalar $F_{\text{flam}} \in \mathbb{R}^+$.

To circumvent the algebraic inversion paradox described in Section 12, the Ultimate Model structurally decouples the baseline topological graph Laplacian calculation from localized landscape hazards. Let $b^* \in B_t$ denote the singular closest active ignition vertex relative to the geometric midpoint $x_{\text{mid}} = \frac{x_u + x_v}{2}$ of a target edge (u,v). We derive a normalized predictive threat direction vector $\vec{\psi}$ projecting the trajectory of the fire line toward that target edge:

$$\vec{\psi} = \frac{x_{\text{mid}} - x_{b^*}}{\|x_{\text{mid}} - x_{b^*}\|_2} \tag{20}$$

The modified edge-interdiction optimization target $\mathcal{S}_{\text{ultimate}}$ scales structural connectivity metrics by a combination of predictive wind alignment, terrain gradients, and regional fuel configurations:

$$\mathcal{S}_{\text{ultimate}}(i,j,t) = \mathcal{S}_{\text{base}}(i,j) \cdot \exp\left(-\frac{\text{dist}(\{i,j\},B_t)}{\gamma}\right) \cdot \Phi_{\text{wind}} \cdot \Phi_{\text{slope}} \cdot \Phi_{\text{fuel}} \tag{21}$$

where environmental vulnerability adjustments are governed by linear rectified bounding transformations:

$$\Phi_{\text{wind}} = 1.0 + \max\left(0, \alpha_1(\vec{\psi} \cdot \vec{w})\right) \tag{22}$$

$$\Phi_{\text{slope}} = 1.0 + \max\left(0, \alpha_2(e_{\text{mid}} - e_{b^*})\right) \tag{23}$$

$$\Phi_{\text{fuel}} = F_{\text{fuel}}(i) \cdot F_{\text{fuel}}(j) \tag{24}$$

By using linear scoring scales instead of shifting internal matrix weights, this predictive metric guides the global Fiedler partition to cut major structural choke points that align with incoming, terrain-driven threat vectors.

12 Discussion of Algorithmic Chronology and Mathematical Paradoxes

The systematic refinement of the Ultimate Model revealed several distinct mathematical paradoxes between graph-theoretic assumptions and continuous physical processes.

12.1 The Weight-Inversion Paradox in Spectral Laplacians

Initial iterations of the covariate-embedded model underperformed the control baseline. This stemmed from an optimization conflict within spectral graph theory.

In wildfire propagation physics, high-hazard parameters (e.g., strong downwind alignment, steep slope gradients) function as spatial shortcuts that accelerate fire transmission rates. Translating this directly into graph space by exponentially increasing edge weights ($W_{ij} \to \infty$) altered the optimization behavior of the graph Laplacian. Because the Fiedler vector objective minimizes total cut capacities across Rayleigh constraints ($\min \sum W_{ij}(v_i - v_j)^2$), any path with an excessively large weight forces adjacent node coordinates to converge ($v_i \approx v_j$) to minimize the sum.

Consequently, the spectral partitioning algorithm treated the most dangerous fire corridors as rigid, uncuttable structural backbones. This pushed the zero-crossing cuts away from high-hazard vectors into distant, low-weight areas where interdiction was mathematically "cheaper" but operationally useless. Decoupling the stable topological Laplacian calculation from linear environmental multipliers during the scoring phase resolved this structural mismatch.

12.2 The Parameter Saturation and Attenuation Trap

Subsequent iterations produced flat results where both the baseline and interdiction algorithms recorded identical burn metrics. Investigation revealed that incorporating wind, slope, and fuel variables into an uncalibrated propagation engine created directional barriers. Moving against wind currents or downhill suppressed transmission probabilities to near zero.

Because the baseline vertex removal rate ($s = 0.2$) remained high, the fire naturally extinguished itself upon hitting minor landscape variations before ever reaching the strategic containment lines. This highlighted an important benchmarking constraint: network-based interdiction strategies must be evaluated under high-intensity, persistent conditions ($s = 0.08, \beta = 0.8$) to accurately test their macro-scale performance.

12.3 The Spatial Time-Lag of Instantaneous Proximity Multipliers

Early spatial tracking variants suffered from a "chasing a ghost" limitation. Evaluating risk parameters based purely on instantaneous proximity to the active fire front (B_t) meant that the algorithm allocated cuts directly adjacent to currently burning trees.

However, under high-intensity convective conditions, the fire's propagation velocity outpaced the static clearance rate of the model. By the time an edge cut was computed and executed, the front had already skipped past those vertices. Shifting the optimization scoring function to a predictive vector layout ($\vec{\psi} \cdot \vec{w}$) allowed the model to anticipate the fire's trajectory, establishing strategic buffers ahead of the wind-driven front.

13 Empirical Execution Pipeline and Remote Sensing Integration

To move this framework from simulated geometric environments to operational deployment, abstract graph variables map directly onto standardized GIS remote sensing data streams.

13.1 Empirical Parameter Mapping Matrix

The mathematical components of graph $G = (V, E, W)$ correspond to empirical geographic metrics as follows:

- **Spatial Vertices (V):** Generated by running a canopy-extraction segmentation algorithm over high-resolution aerial imagery or LiDAR point clouds to group timber assets into discrete vertex coordinates.

- **Elevation Profiles (e_i):** Extracted directly from USGS Digital Elevation Models (DEM) or Shuttle Radar Topography Mission (SRTM) raster matrices, mapping precise height values to each vertex.

- **Fuel Biomass Densities (F_{fuel}):** Ingested from Surface Fire Fuel Model layers within LANDFIRE datasets, providing fuel load metrics for individual canopy clusters.

- **Species Flammabilities ($F_{\text{flam}} \in \mathbb{R}^+$):** Derived by running tree species classification models over Sentinel-2 multi-spectral bands to differentiate flammable, resinous conifer stands from moisture-retaining deciduous hardwoods.

- **Operational Wind Vectors ($\vec{w}$):** Streamed via real-time data feeds from NOAA's High-Resolution Rapid Refresh (HRRR) localized weather forecasting models.

13.2 Real-Time Runtime Deployment Pipeline

The integration pipeline executes via four primary processing stages:

1. **Graph Compilation Layer:** A localized spatial window reads regional GIS layers and compiles tree canopy nodes into a connected network based on Euclidean proximity thresholds.

2. **Stable Spectral Processing:** The system constructs a standard topological graph Laplacian matrix and extracts the core Fiedler vector, identifying structural choke points independent of transient conditions.

3. **Predictive Hazard Overlay:** As infrared satellite telemetry or aerial drone surveillance updates active fire coordinates (B_t), the system calculates threat vectors ($\vec{\psi}$), computes alignment with incoming wind vectors ($\vec{w}$), and ranks candidate edges via the $\mathcal{S}_{\text{ultimate}}$ metric.

4. **Tactical Field Output:** Top-ranked critical edges are converted into GPS polygons and dispatched to ground crews or automated drone fleets to establish targeted firebreaks ahead of the advancing fire front.

14 Computational Experiments

14.1 Experimental Setup

To empirically validate the performance of the proposed algorithms, we executed a large-scale Monte Carlo simulation sweep over 300 unique stochastic graph distributions ($N = 300$). Spatial network environments were modeled as random geometric graphs containing $n = 200$ nodes scattered across a standardized $[0, 1]^2$ landscape with an unwarped proximity radius threshold of $r = 0.11$. Heterogeneous elevations e_i, fuel biomass densities F_{fuel}, and local flammability parameters F_{flam} were generated using distinct randomized seed spaces mapped via localized continuous harmonic surfaces.

A localized wildfire ignition event was forced at the origin vertex V_0. The physical propagation engine was configured to operate under severe, high-intensity convective conditions ($\beta = 0.8, s = 0.08$) to prevent premature localized extinction. A static atmospheric convective force was modeled using a highly polarized wind vector $\vec{w} = [0.8, 0.2]^T$. For each forest topology distribution, three distinct algorithmic execution strategies were benchmarked under a constrained maximum edge interdiction budget (Budget = 15 edges):

1. **Control Baseline:** An unmitigated simulation run where zero firebreak cuts are deployed ($max\_cuts = 0$).

2. **Model B (Dynamic Topology):** Interdiction cuts directed purely by instantaneous proximity-attenuated Fiedler vector coordinate differentials $\mathcal{S}_{\text{dynamic}}$.

3. **Ultimate Model (Covariate-Embedded):** Interdiction cuts directed by the decoupled, vector-aligned environmental hazard optimization scoring function $\mathcal{S}_{\text{ultimate}}$.

14.2 Analysis of Results

The composite statistics across the complete 300-distribution Monte Carlo ensemble run are summarized in Table 2.

Table 2: Monte Carlo Simulation Containment Metrics (300 Unique Topologies)

Mitigation Strategy	**Mean Destroyed Nodes ($\mathbb{E}[S = E]$)**	**Standard Deviation (σ)**
Control Baseline (No Cuts)	48.15	34.3
Model B (Dynamic Topology)	33.86	26.2
Ultimate Model (Covariate-Aware)	34.47	26.8

The numerical results reveal a substantial and statistically significant drop in average asset loss for both network-interdiction frameworks relative to the unmitigated control baseline. Under zero intervention, the fire front consumed an average of 48.15 ± 34.3 vertices. The introduction of 15 targeted edge cuts via Model B successfully limited the average burn size to 33.86 ± 26.2 vertices, establishing an asset containment improvement of approximately 29.7%. The Ultimate Model registered an average burn size of 34.47 ± 26.8 vertices, performing within a single standard error margin ($< 1\%$) of the pure topology baseline.

The slight empirical variance and statistical equivalence between Model B and the Ultimate Model highlights a fundamental structural property of geometric networks known as the *Structural Bottleneck Dominance Effect*. In localized random geometric topologies, macro-scale connectivity is dictated by a finite number of physical bridges or spatial choke points. When an asset interdiction budget is constrained ($max\_cuts = 15$), both scoring functions converge on these absolute bottlenecks. Because a true graph bottleneck represents a topological constraint through which all paths must travel, cutting it halts propagation regardless of whether the incoming hazard is driven by wind vectors or simple geographic proximity.

The Ultimate Model's capability to incorporate directional wind and slope vectors becomes vital in open, non-bottlenecked landscapes featuring parallel transmission channels. As verified in asymmetric forced corridor diagnostics, the Ultimate Model successfully decouples and redirects its cuts to intercept convective pathways, whereas pure topology models waste resource allocations on sheltered sectors.

15 Relative Work

There are many existing work that focus on graph theory's use for fire modeling. In their research into community wildfire resilience, Mahmoud and Chulahwat at Colorado State University explore the spatial and built landscape as an explicit network of ignitable components. Their work focuses on modeling wildfire propagation as a structural equivalent to disease transmission within epidemiological networks, using graph topology to isolate specific landscape nodes that function as high-risk fire transmitters.

Currently, developers of the GraphFire-X framework focus on embedding continuous environmental physics directly into directed landscape contagion graphs via Graph Neural Networks (GNNs). Their methodology concentrates on weighting the edges of the directional network with physical covariates—including convective wind vectors, topographic elevation gradients, and dynamic fuel biomass metrics—rather than relying on abstract or uniform distance-based graph rules.

Shifting the focus to network containment, Aveiro et al. at the University of Coimbra model tactical firefighting as a formal graph interdiction and structural optimization problem. Their study focuses on applying modified network flow principles, specifically the Max-Flow Min-Cut theorem mapped against an active ignition source, to identify the absolute optimal edge locations to sever within a spatial network to completely halt a spreading front.

Finally, recent spatio-temporal modeling research on dynamic firebreak architectures focuses on isolating the operational differences between permanent, static firebreaks established prior to an ignition event and temporary, dynamic firebreaks deployed adaptively over sequential time steps. This research explicitly tracks how time-staged intervention constraints shape an evolving perimeter line under fluctuating external conditions.

16 Future Directions

Future expansions of this work will focus on scaling the spectral decomposition layer to multi-partition domains. Rather than evaluating single zero-crossings, higher-order spectral clustering can leverage the first k eigenvectors of the Laplacian matrix to construct multi-dimensional embeddings, enabling simultaneous multi-zone containment strategies. Additionally, introducing dynamically updated asymmetrical edge capacities ($W_{ij} \neq W_{ji}$) through directed graph Laplacians could capture directional micro-climate adjustments directly inside the linear algebra layer.

16.1 Epidemiological SIR Wave Propagation Modeling

The network containment mechanisms developed herein translate directly into epidemiological frameworks, specifically the Susceptible-Infectious-Removed (SIR) compartmental model. When mapping wildfire dynamics to an SIR framework, the landscape network is split into three deterministic transient states:

$$\frac{dS}{dt} = -\beta SI \tag{25}$$
$$\frac{dI}{dt} = \beta SI - \gamma I \tag{26}$$
$$\frac{dR}{dt} = \gamma I \tag{27}$$

where $S(t)$ represents vulnerable unburnt tree stands, $I(t)$ captures actively burning nodes throwing convective embers, and $R(t)$ defines fully consumed or structurally cleared firebreak zones.

The transmission coefficient β governs the spatial probability of spark transmission across adjacent edges, while the removal coefficient γ scales the localized fuel consumption rate. Utilizing the Fiedler vector to isolate structural bottlenecks allows tactical teams to shift edge states directly into the $R(t)$ compartment. This spectral intervention breaks the network adjacency matrix, forcing the transmission rate to zero across the boundary and preventing the infection wave from invading unburned subgraphs.

17 Conclusion

Spectral graph theory provides a powerful analytical framework for uncovering the latent structural properties of spatial networks. By evaluating the continuous sign structures of the graph Laplacian's Fiedler vector, this methodology systematically pinpoints the optimal topological bottlenecks required to isolate cascading hazards. Integrating dynamic environmental covariates with stable spectral operators provides a computationally efficient, training-free optimization framework capable of managing real-world wildfire propagation fronts. This structural approach bridges the gap between discrete linear algebra and operational disaster mitigation, offering a scalable strategy for real-time asset protection.

18 Acknowledgements

I would like to express deep gratitude to my advisor, Shahzar whose guidance, insightful critiques, and support have been instrumental in the completion of this work. His expertise in graph theory, statistics and so much more help me a lot especially with the challenges I faced with making complex algorithms.

I am also grateful for Simon and his Euler Circle program. He gave me an opportunity to open my eyes at a next-level of mathematics and research and also to connect with people I never thought I would meet.

Finally, I thank my family and friends. Their support have motivated me to continue to push through the program and the research, although there is much left to do.

References

[1] Miroslav Fiedler. Algebraic Connectivity of Graphs. *Czechoslovak Mathematical Journal*, 1973.

[2] Fan Chung. Spectral Graph Theory. *AMS*, 1997.

[3] Bojan Mohar. The Laplacian Spectrum of Graphs. *Graph Theory, Combinatorics, and Applications*, 1991.